BIOCHEMISTRY
including biophysical chemistry & molecular biology
Article

Biochemistry **2009,** *48,* 7927–7938 7927
DOI: 10.1021/bi900776u

Macromolecular Interaction of Halichondrin B Analogues Eribulin (E7389) and ER-076349 with Tubulin by Analytical Ultracentrifugation†

P. Holland Alday and John J. Correia*

Department of Biochemistry, University of Mississippi Medical Center, Jackson, Mississippi 39216

Received May 5, 2009; Revised Manuscript Received July 6, 2009

ABSTRACT: Halichondrin B is an antimitotic drug that inhibits microtubule assembly. To understand the molecular details of its interaction with tubulin, we investigated the binding of two halichondrin B analogues, eribulin (previously, ER-086526, E7389) and ER-076349, to tubulin by quantitative analytical ultracentrifugation. Eribulin is currently undergoing phase III clinical trials for cancer; ER-076349 is a closely related analogue with C.35 hydroxyl instead of C.35 primary amine [Towle, M. J., et al. (2001) *Cancer Res. 61*, 1013]. Below the critical concentration for microtubule assembly and in the presence of GDP, tubulin undergoes weak self-association into short curved oligomers. Eribulin inhibits this oligomer formation 4−6-fold, while ER-076349 slightly stimulates oligomer formation by 2-fold. This is in contrast to vinblastine which strongly stimulates large spiral polymers by 1000-fold under these same conditions. Vinblastine-induced spiral formation is strongly inhibited by both eribulin and ER-076349. Colchicine binding to the intradimer interface has no significant effect on small oligomer formation or the inhibitory activity of eribulin on this process. These results suggest that halichondrin B analogues bind to the interdimer interface or to the β-subunit alone, disrupt polymer stability, and compete with vinblastine-induced spiral formation. Stathmin is known to form a tight 1:2 complex with tubulin. Eribulin strongly inhibits formation of the 1:2 stathmin−tubulin complex (>3.3 kcal/mol), while ER-076349 weakens formation of the 1:2 complex by ~1.9 kcal/mol. These results suggest that eribulin is a global inhibitor of tubulin polymer formation, disrupting tubulin−tubulin contacts at the interdimer interface. ER-076349 also perturbs tubulin−tubulin contacts, but in a more polymer specific manner, reflecting adaptability of the interdimer interface to drug and polymer polymorphism. These results suggest halichondrin B analogues exhibit unique tubulin-based activities that may underlie the clinical utility of these compounds.

Many of the antimitotic drugs that interact with tubulin and microtubules and cause G2/M arrest are also known to induce assembly of tubulin into either less dynamic microtubule polymers or nonmicrotubule polymers (*1*, *2*). These drugs fall into three broad classes of site specific binding. The classic example of microtubule stabilization is the taxane class of antimitotics (including paclitaxel, taxotere, epothilones A and B, eleutherobin, and discodermolide), which bind between protofilaments in the microtubule lattice at the M-loop on the β-subunit and stabilize lateral contacts between protofilaments, thus stabilizing the microtubule lattice (*3*−*5*). Members of the colchicine class of antimitotics (including colchicine, colcemid, podophyllotoxin, nocodazole, noscapine, combretastatin, and staganacin) bind at the intradimer interface between the α- and β-subunits (*6*). This class of compounds typically causes tubulin heterodimer sequestering, substoichiometric microtubule poisoning, and microtubule depolymerization, although assembly into sheetlike polymers and small oligomers has been reported (*1*, *7*). The vinca alkaloid class of antimitotics (including the clinically useful drugs vinblastine, vincristine, vinorelbine, and vinflunine, as well as dolastatin 10) bind at the interdimer interface (*8*) and cause microtubule depolymerization while inducing spiral and ringlike polymer formation. Halichondrin B and analogues are thought to compete for vinblastine binding and in general have been thought to act by a mode of action similar, although not identical, to that of vinca alkaloids (*9*−*15*).

The in vitro techniques used to ascertain the mode of action of antimitotic drugs include turbidity, electron microscopy, and analytical ultracentrifugation (*16*, *17*). The advantage of analytical ultracentrifugation (AUC)[1] is the ability to extract the mode of molecular interaction, the stoichiometry, and the energetics of the process, i.e., the equilibrium constants for the molecular mechanism (*1*, *16*−*20*). Here we investigate the interaction of two halichondrin B analogues, eribulin (previously ER-086526, E7389) and ER-076349 (*13*), with tubulin by quantitative AUC methods. Structures of halichondrin B, eribulin (as its mesylate salt), and ER-076349 are presented in Figure 1. Surprisingly, and unlike vinca alkaloids, these analogues appear to either suppress or have minimal effects on tubulin nonmicrotubule polymer assembly. Furthermore, they compete for and suppress vinblastine-induced spiral formation and the interaction of tubulin with stathmin. The different modes of drug−tubulin interaction exhibited by eribulin and ER-076349, between themselves and

†Supported by Eisai Research Institute of Boston, Inc. (Andover, MA).
*To whom correspondence should be addressed. Phone: (601) 984-1522. Fax: (601) 984-1501. E-mail: jcorreia@biochem.umsmed.edu.

[1]Abbreviations: AUC, analytical ultracentrifugation; EGTA, [ethylene bis(oxyethylenenitrilo)]tetraacetic acid; GDP, guanosine 5′-diphosphate; GTP, guanosine 5′-triphosphate; MAP, microtubule-associated protein; PC-tubulin, MAP-free phosphocellulose-purified tubulin; Pipes, piperazine-*N*,*N*′-bis(2-ethanesulfonic acid); rmsd, root-mean-square deviation; TCEP, tris(2-carboxyethyl)phosphine hydrochloride.

Published on Web 07/08/2009

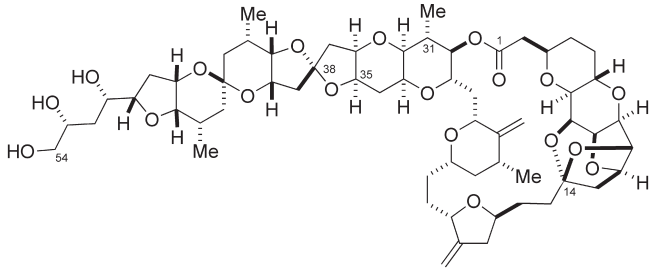

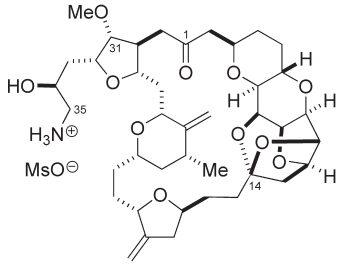

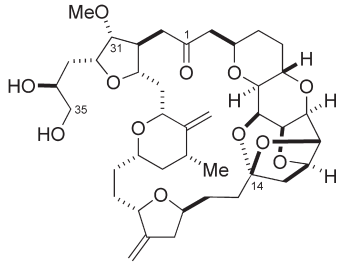

FIGURE 1: Structures of halichondrin B, ER-076349, and eribulin (shown as a mesylate salt).

relative to other tubulin-targeted agents, may have implications for the preclinical spectrum of in vitro and in vivo anticancer activities seen with these agents (*13*, *14*), as well as the potential clinical utility of halichondrin B-based chemotherapeutic agents in cancer patients.

MATERIALS AND METHODS

Tubulin Purification. MAP-free pig brain tubulin (PC-tubulin) was obtained by two warm−cold polymerization−depolymerization cycles followed by phosphocellulose chromatography to separate tubulin from MAPs (*21*, *22*). Protein concentrations were determined spectrophotometrically (*23*) (ε_{278} = 1.2 mL mg^{-1} cm^{-1}). Experiments were performed in P80 [80 mM Pipes, 1 mM $MgSO_4$, 2 mM EGTA, 0.1 mM TCEP, and 50 μM GDP (pH 6.9)]. Tubulin samples were equilibrated into the appropriate buffer by a spun column technique utilizing G-50 fine (*16*, *24*).

Eribulin and ER-076349 Solutions. The halichondrin B analogues eribulin (supplied as its mesylate salt, MW = 826.00) and ER-076349 (MW = 730.88) were provided by Eisai Research Institute (*13*, *14*). Eribulin and ER-076349 lack a UV absorbance, and thus, all stock solutions were made up by weight into >99.9% DMSO (Sigma). Both the drug and the DMSO were measured by weight. Stocks were typically 30−40 mM or 20× dilutions of these stocks, and drug was added directly to each tubulin solution to make the final total drug concentration. Final DMSO concentrations were typically 0.36% and always <0.5% unless DMSO was the experimental variable. Since eribulin is a mesylate (methanesulfonic acid) salt, control AUC runs were conducted in 56.5 μM methanesulfonic acid (Aldrich, catalog no. 471356), derived from a stock solution in DMSO, to rule out a direct role for methanesulfonic acid in the observed inhibitory activity.

Colchicine−Tubulin Complex. Tubulin was incubated with 2 mM colchicine for 60 min at 20 °C and passed over a spun column to remove unbound colchicine and equilibrate the complex with P80. Spectra were recorded on these samples at 278 and 354 nm to ascertain the colchicine:tubulin binding ratio (colchicine ε_{354} = 16600 M^{-1} cm^{-1}) which was found to be consistently 0.9 mol/mol for these conditions. The protein complex was diluted to various concentrations and run in sedimentation velocity experiments in the presence and absence of 28 μM eribulin. The colchicine complex was made fresh before each experiment. Since colchicine binding is known to be slowly reversible (*25*), irreversible on the time scale of the velocity experiment, these experiments test the assumption that colchicine and eribulin bind to different sites on tubulin.

Tubulin−Vinblastine Experiments. The interaction of vinblastine with tubulin has been studied extensively via AUC techniques by our laboratory (*17*, *18*, *26*−*28*). Tubulin was equilibrated into P80 (*16*, *24*), diluted to 5 μM with 20 μM vinblastine, and spun at 30K rpm at 19.7 °C, and data were collected at 278 nm. Data were analyzed with DCDT^{+2} to produce $g(s)$ distributions (*29*) (see Figure 4). When prepared this way, the vinblastine-induced spirals sediment at 25.20 ± 0.91 s, the variation being primarily due to small differences in protein concentration. This tubulin−vinblastine mixture was then titrated with increasing amounts of eribulin (from 2.8 to 28.3 μM) or repeated with ER-076349 (from 0.8 to 67.0 μM) and spun in the XLA to determine the effect on spiral polymer size distributions. The speed has to be adjusted to vary the number of scans collected to perform proper DCDT^{+2} $g(s)$ analysis. As described above, tubulin−vinblastine samples were prepared fresh for each set of experiments.

Stathmin−Tubulin Experiments. A stathmin−eGFP gene (MW = 44945) with a single Ala linker at the C-terminus was cloned into a Novagen pET-11d vector and used to transform pLysS *Escherichia coli* containing the Rosetta plasmid. Expression was induced with 0.5 mM IPTG and allowed to continue for 4 h at 18 °C, at which time cells were harvested and the pellet was frozen overnight. After lysis by sonication on ice, cell debris was removed by centrifugation (Sorvall SE3, 20K rpm, 4 °C, 20 min). Purification of the stathmin−eGFP construct proceeded via a modified version of the method used by Fukuda (*30*). Differential precipitation with 20 and 70% $(NH_4)_2SO_4$ produced a pellet that

was solubilized in minimal GFP resuspension buffer. This was fractionated over a Sephacryl-300 HR column (Pharmacia). Fractions were assayed for purity spectroscopically and via SDS−PAGE. Appropriate fractions were pooled and loaded onto a DEAE column, washed with GFP resuspension buffer [20 mM Tris and 0.1 mM TCEP (pH 7.5)], and eluted with a NaCl gradient from 0 to 1 M. After another assay for purity, appropriate fractions were concentrated with 70% $(NH_4)_2SO_4$, resuspended in minimal GFP resuspension buffer, and stored at −80 °C.

Both the stathmin−GFP construct and tubulin were equilibrated into P80 buffer with spin columns and mixed to a give a Tb:St ratio of ~1.2. The samples were split, and drug was added to produce mixtures with 0−113 μM eribulin and 0−134 μM ER-076349. Samples were run at 42K rpm and 19.7 °C, and data were collected at 278 and 488 nm to allow selective tracking of stathmin, tubulin, and the $StTb_2$ complex. (Note that data collected at 488 nm are unique to the stathmin−GFP construct while 278 nm data track both tubulin and the GFP portion of the stathmin−GFP construct.) Data were analyzed with DCDT^{+2} to produce $g(s)$ distributions (*29*) and quantitatively analyzed with Sedanal (*31*) to an ABCD model involving formation of a weak 1:1 StTb complex and a tight 1:2 $StTb_2$ complex.

$$St + Tb \leftrightarrow StTb \quad K_1$$

$$StTb + Tb \leftrightarrow StTb_2 \quad K_2$$

Detailed AUC analysis (to be presented elsewhere) has shown K_1 is weak (~10^4 M^{-1}) while K_2 is a tight nucleotide- and pH-dependent parameter (~10^8 M^{-1}). Fitting in the presence of drug was thus done to a $K_{2,app}$ value holding K_1 constant, to measure the apparent weakening of the $StTb_2$ complex.

Sedimentation Velocity Experiments. Sedimentation studies were performed in a Beckman Optima XLA analytical ultracentrifuge equipped with absorbance optics and an An60 Ti rotor at 19.7 °C. Temperature was calibrated as described previously (*32*). Velocity data were typically collected at the appropriate speeds using 278 nm at a spacing of 0.002 cm with one flash at each point in a continuous-scan mode. Below 1 OD, samples were run in 1.2 cm centerpieces; above 1 OD and up to ~5 OD, samples were run in 0.3 cm centerpieces. In experiments with the stathmin−GFP construct, data were collected at 278 and 488 nm. All experiments were initially analyzed with DCDT^{+2} to produce $g(s)$ distributions and weight-average S values ($\hat{S}_w$) (*29*). Quantitative analysis of $\hat{S}_w$ data (*26*) or boundary shape (*31*) involves fitting to a model for indefinite polymerization (either tubulin alone or ligand-mediated polymer growth) where K_{iso} is the propagation constant for polymer growth in the presence or absence of drug (V for vinca alkaloid; see refs (*26*−*28*) for details).

$$Tb + Tb_n \leftrightarrow Tb_{n+1} \quad K_{iso}$$

$$TbV + (TbV)_n \leftrightarrow (TbV)_{n+1} \quad K_{iso}$$

Analysis with Sedanal requires input of molecular weight (MW), extinction coefficients, and density increments (typically estimated from 1-$\nu\rho$ values). The MW of tubulin is fixed at 100000, and the MW of the stathmin−GFP construct is fixed at 44945. The P80 solution density was measured in an Anton Paar DMA 5000 instrument to be 1.01360 g/mL at 19.7 °C. The ν_{bar} of tubulin was taken from the literature [0.736 (*33*, *34*)], and the ν_{bar} of the stathmin−GFP construct was estimated with Sednterp (*35*) to be 0.7354. The extinction coefficient of tubulin at 278 nm is 1.2 mL mg^{-1} cm; the extinction coefficient of the stathmin−GFP construct at 278 nm is 0.487 mL mg^{-1} cm. The extinction coefficient of the stathmin−GFP construct at 488 nm varies from preparation to preparation [due to GFP folding efficiency and pH dependence (*36*, *37*)] and is measured in a sedimentation velocity experiment performed at three concentrations of the stathmin−GFP construct alone by constraining the concentration of the 488 nm data to the concentration of the 278 nm data. Within Sedanal, one assumes the stathmin concentrations must be identical in the data collected at different wavelengths and fits for ε_{488} relative to ε_{278}. In the preparation used in these experiments, the stathmin ε_{488} equalled 0.933 mL mg^{-1} cm.

RESULTS

Tubulin undergoes Mg^{2+}- and nucleotide-dependent oligomerization under conditions that do not favor microtubule assembly (*27*). This serves as a baseline reaction for proper interpretation of all other association reactions that might occur in a drug-dependent manner. This oligomer formation is demonstrated by the $g(s)$ sedimentation coefficient distributions shown in Figure 2A. With increasing tubulin concentrations (as indicated by the area under each curve), the distribution shifts to higher S values, consistent with concentration-dependent formation of small oligomers. Additional experiments demonstrate that up to 0.5% DMSO or the presence of a tubulin−-colchicine complex has no significant qualitative effect on this reaction. Figure 2B shows the effect of titrating increasing amounts of eribulin (from 0 to 112.6 μM) into a fixed concentration of tubulin (~4 μM). Rather than induce oligomer or spiral formation, the drug induces the boundary to shift to slower S values with an average $\hat{S}_w$ value of 5.09 ± 0.05 S ($S_{20,w}$ = 5.36 S). At this tubulin concentration, this is 3.1% slower than the expected sedimentation behavior of tubulin in the absence of eribulin and thus well below the uncertainty in the method. The DMSO control experiment in Figure 2A rules out an effect due to a trivial change in solution density or viscosity or a direct effect of DMSO alone. (Above 0.5% DMSO, the boundary slows due to increased solution viscosity.) Plotting of the weight-average or $\hat{S}_w$ values versus protein concentration [Figure 2C (○)] and repeating the experiment at other tubulin concentrations (<10 μM) reveal that the average $\hat{S}_w$ value observed in the presence of 56.5 μM eribulin corresponds to the value for tubulin alone when data are extrapolated to zero protein concentration (see intercepts at zero protein concentraion). The sedimentation behavior induced by eribulin thus corresponds to the S_o value for the tubulin heterodimer under these solution conditions. Direct boundary fitting of the data at tubulin concentrations of < 10 μM with Sedanal are consistent with a noninteracting system comprised of tubulin heterodimer and a small amount (3%) of tubulin aggregate (data not shown). Thus, the conclusion is that eribulin binds to tubulin and suppresses oligomer formation. The mechanism may involve sequestering a nonpolymerizable heterodimer or binding and destabilizing the interdimer interface by a direct or an allosteric effect (*15*). To test this hypothesis, eribulin experiments were repeated in a 3 mm centerpiece with a protein concentration of up to ~30 μM. Those data are plotted in Figure 2C (☆) and show a slight increase in $\hat{S}$w with increasing tubulin concentrations. This trend suggests a higher tubulin concentration can shift the equilibrium back toward oligomer formation in the presence of

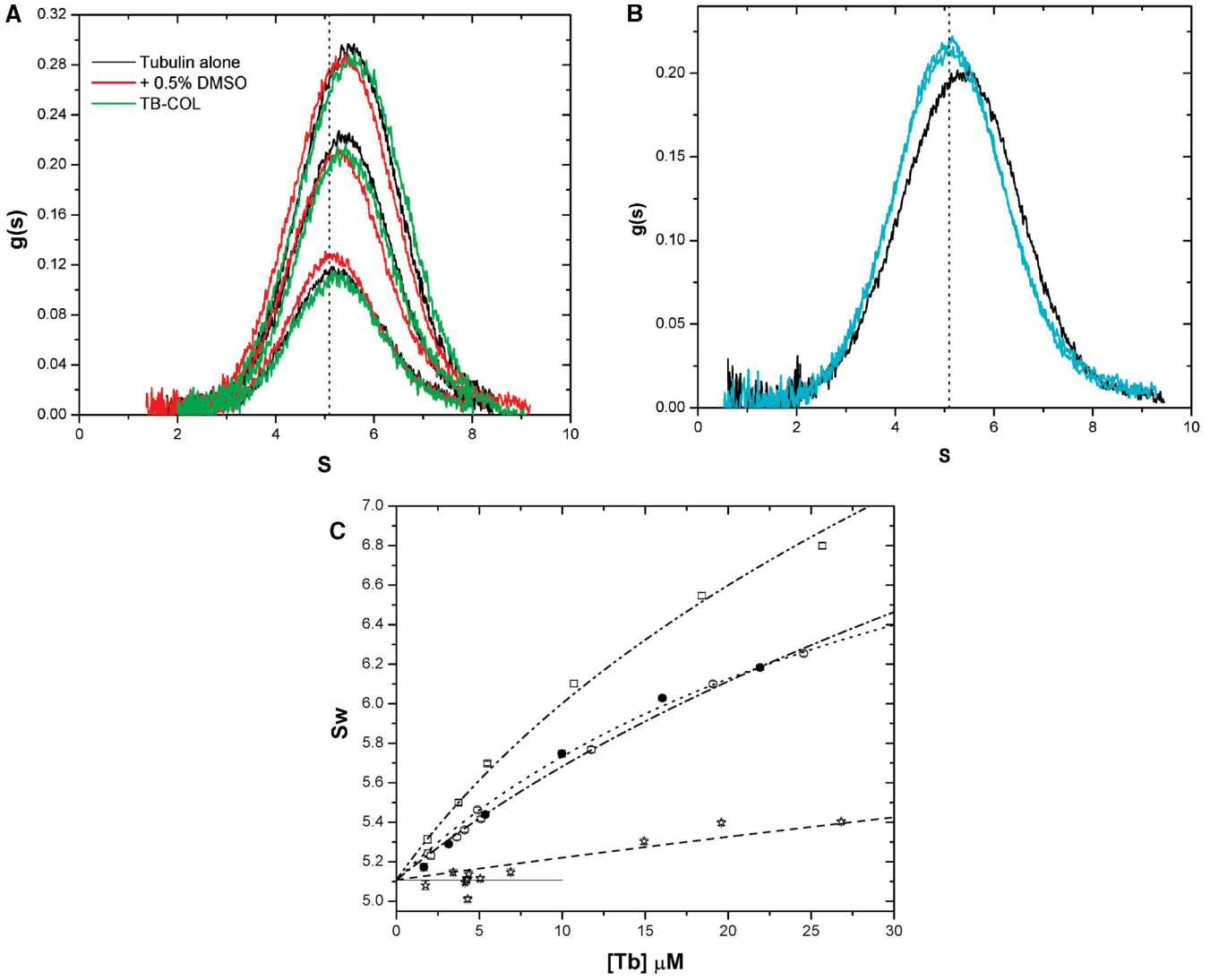

FIGURE 2: Sedimentation velocity analysis of tubulin as a function of concentration and drug. (A) DCDT^{+2} $g(s)$ analysis of (black) tubulin at 2, 4, and 6 μM in 80 mM Pipes, 1 mM $MgSO_4$, 2 mM EGTA, 0.1 mM TCEP, and 50 μM GDP (pH 6.9) (P80), (red) tubulin in P80 with 0.5% DMSO, and (green) the tubulin−colchicine complex in P80 all run at 42K rpm and 19.7 °C. Note the shift to higher S values with increasing protein concentrations. The vertical line at 5.09 s represents extrapolation to zero protein concentration. The superposition of the three data sets demonstrates these variables have no significant effect on oligomer formation (also see Table 1). (B) Tubulin at 5 μM in P80 in the absence of drug (black) or 3.25 and 112.6 μM eribulin (teal). Note the left shift in S values in the presence of eribulin to an S_w of 5.09 ± 0.05 S, indicated by the vertical line, the average from five drug concentrations (3.25, 6.5, 28.2, 56.3, and 112.6 μM). Even at substoichiometric drug levels (3.25/5), the association reaction is suppressed. (C) Weight-average S values plotted vs tubulin concentration for tubulin alone (○), tubulin with 56.5 μM methanesulfonic acid (●), tubulin with 56.5 μM eribulin (*), and tubulin with 67 μM ER-076349 (□). The lines are fits of the weight-average S_w data to an isodesmic model using a curved oligomer model for each species S_n (*24*−*26*). K_{iso} values are summarized in Table 1. The horizontal solid line is the average S_w for all the eribulin data below 10 μM (5.107 S).

eribulin, but eribulin clearly weakens oligomer stability.[2] Thus, unlike vinca alkaloids, eribulin does not stimulate large non-microtubule polymer formation but rather binds to tubulin and suppresses or weakens oligomer formation.

Previous work in this area concluded noncompetitive binding occurs between vinca alkaloids and halichondrin B and its analogues (*9*, *11*, *12*, *15*) and concludes they bind to the same interdimer domain in nonoverlapping sites, termed the vinca domain. Many of the drugs that bind to this domain induce oligomers, while some appear to suppress oligomer formation and sequester tubulin in a nonpolymerizable complex. The field understands the complexity of this class of drugs as being due to binding at the same domain, binding at overlapping sites, or binding at allosteric sites. Thus, consistent with the sedimentation data, we must also consider mechanisms that allow for sequestering, binding to the same site, or binding to an allosteric site. To test these possibilities, we first performed eribulin experiments on the tubulin−colchicine complex. Since colchicine binds irreversibly to tubulin in the time frame of the experiment (*25*), in the presence of the preformed colchicine complex, eribulin will not be able to fill the colchicine site. Figure 3 shows, in the presence of colchicine, eribulin still induces a shift to lower S values, consistent with suppression of oligomer formation. Thus, eribulin does not bind to the colchicine site, the intradimer interface, but rather is able to bind to the tubulin−colchicine

[2]We cannot exclude the slight possibility this may partially be a concentration-dependent competition between free tubulin oligomer formation and eribulin binding to tubulin heterodimers. This alternate interpretation depends upon the affinity of eribulin for tubulin since tight affinity produces stoichiometric binding and precludes the presence of free tubulin. The rest of the experimental data seems to favor weak eribulin-induced oligomer formation.

complex at a second site and suppress or weaken oligomer formation.

We next tested the ability of the structurally related halichondrin B analogue ER-076349 to bind to tubulin and induce oligomer formation. ER-076349 has antiproliferative potency and ability to induce G2/M arrest roughly comparable to those of eribulin (*13*), although mitotic blocks induced by ER-076349 are moderately reversible while those induced by eribulin are irreversible (*14*). The AUC results for ER-076349 are shown in Figure 2C (□) and reveal that ER-076349 slightly enhances the formation of tubulin oligomers, although this effect is dramatically weaker than the effect of vinblastine (*17*, *18*) (see below). This supports an interpretation whereby the existence of C.35 hydroxyl (ER-076349) instead of C.35 primary amine (eribulin) enables ER-076349 to insert into either the interdimer interface or an allosteric site and slightly stabilize small tubulin oligomers. Energetically, the primary amine in eribulin may contribute a repulsive force that prevents or weakens binding to the interdimer interface. [This is in contrast to the polar repulsive force exerted by inserting double F substitutions in the vinca alkaloid analogue vinflunine that also weaken spiral formation (*38*).]

These AUC data on tubulin self-association can be quantified in two ways. Weight-average $\hat{S}_w$ data collected as a function of protein concentration can be fit to an indefinite polymerization model as described in previous work from our lab (*17*, *18*, *26*−*28*). The results of weight-average analysis are summarized in Table 1 with the best-fit lines appearing in Figure 2C. Relative to tubulin alone, eribulin suppresses tubulin self-association at least ~6-fold (see Discussion), while ER-076349 enhances association 2-fold. Alternatively, these data can be directly fit with Sedanal which simulates and fits the shape of the reaction boundary during sedimentation (*27*, *31*). These results also appear in Table 1 and are in general consistent with the $\hat{S}_w$ fitting results. Direct boundary fitting with Sedanal is in principle more discriminating and robust, but when the fitting model is appropriate, both analysis methods give similar quantitative conclusions (*27*, *28*).

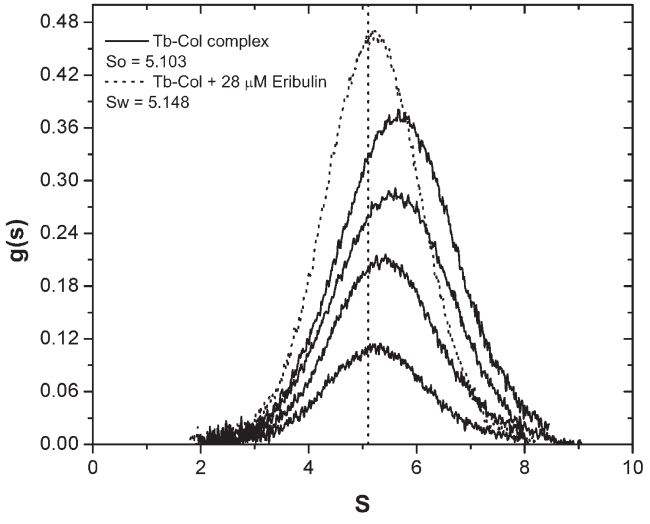

FIGURE 3: Sedimentation velocity analysis of the tubulin−colchicine complex in the absence and presence of 28 μM eribulin. Data were collected at 42K rpm and 19.7 °C and analyzed with DCDT^{+2}. The data for the tubulin−colchicine complex alone are consistent with a concentration-dependent association [2, 4, 6, and 8 μM (—)] that extrapolates back to an S_o value of 5.103 s (vertical dotted line). In the presence of 28 μM eribulin and 8 μM tubulin−colchicine complex, the $g(s)$ distribution (···) shifts to lower S values (S_w = 5.148 S), proving that eribulin does not bind to the colchicine site.

Eribulin's ability to suppress tubulin self-association, while interesting in comparison to the abilities of other vinca binding site drugs, does not seem on the surface to be a dramatic result, especially given the weak 2-fold increase in the level of self-association seen with ER-076349 and the 4−6-fold decrease in the level of self-association seen with eribulin. To further investigate these results, eribulin was added to a solution of vinblastine-induced spirals. The interaction of vinblastine with tubulin has been studied extensively in our laboratory (*17*, *18*, *27*, *28*, *38*). Our focus has been the role of allosteric effectors like pH, Mg^{2+}, and nucleotide content in the energetics of vinca alkaloid-induced spiral polymer formation. In this study, our original hypothesis was that halichondrin B derivatives, eribulin and ER-076349, would strongly induce oligomers and possibly copolymerize with vinca alkaloid spirals. On the basis of the findings described above, however, we now hypothesize that eribulin would compete with vinblastine binding and cause dissociation of the spirals. The results are presented in Figure 4. Tubulin (5 μM) was assembled into spirals in the presence of 20 μM vinblastine, and eribulin was added at concentrations from 1.4 to 28.3 μM. Panel A shows the shift in the sedimentation coefficient distribution to lower $\hat{S}_w$ values with more than half of the dissociation complete at an eribulin:tubulin ratio of <0.25 (Figure 4B). By 28.3 μM eribulin, the sample is approaching the sedimentation behavior of the tubulin heterodimer, similar to the data in Figure 2B. Identical results were obtained with ER-076349 [0.8−67.0 μM (Figure 4A,B)], demonstrating that both of these drugs destabilize vinblastine-induced spirals.

What mechanism explains these results? Vinblastine induces tubulin spiral formation with a propagation constant of 2.3×10^7 M^{-1} (*12*). [This is strictly dependent upon vinblastine concentration through the K_{app} term defined previously for spiral formation (*12*, *13*). At 15−20 μM vinblastine, $K_{app} = 1.0-1.2\ 10^7$ M^{-1}.] Thus, if eribulin sequestered tubulin, a direct competition interpretation implies that eribulin has a tighter affinity for tubulin heterodimers than vinblastine has for tubulin spirals. This

Table 1: K_{iso} Values for Tb Self-Association Derived from Weight-Average (*24*) or Sedanal (*29*) Fitting of the Data[a]

conditions	$\hat{S}_w$ K_{iso}	rmsd (S)	Sedanal K_{iso}	rmsd (OD)
Tb alone	2.005×10^4	0.02315	2.919×10^4 (2.836, 3.005)	0.01134
Tb with 0.5% DMSO	2.975×10^4	0.01044	2.614×10^4 (2.411, 2.823)	0.01112
Tb-COL	3.158×10^4	0.00874	3.417×10^4 (3.306, 3.531)	0.00895
eribulin	0.338×10^4	0.06227	0.866×10^4 (0.821, 0.912)	0.01419
ER-076349	3.444×10^4	0.04749	4.574×10^4 (4.469, 4.680)	0.01086
methanesulfonic acid	2.233×10^4	0.04650	2.523×10^4 (2.461, 2.585)	0.01070

[a] All fits used a 21-bead spiral model as described in ref (*25*). All fits use the same S_o value (see Figure 2C) with hydrodynamic nonideality $g = K_s = 0.018$ mL/mg (*24*, *25*). The K_{iso} value from S_w fitting is used to generate the curves in Figure 2C. The K_{iso} values from Sedanal are reported with a 95% confidence interval.

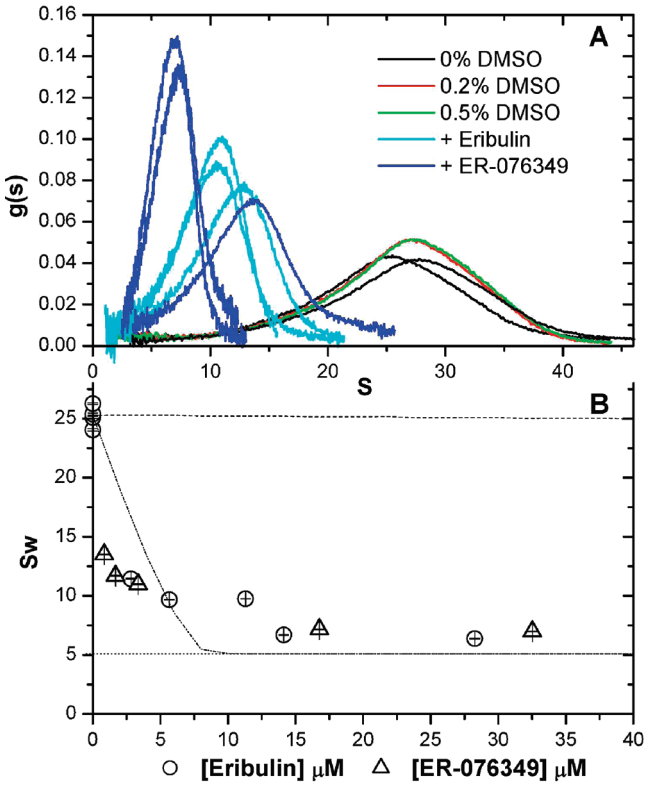

FIGURE 4: Sedimentation velocity analysis of the effect of eribulin and ER-076349 on tubulin vinblastine spiral formation. Tubulin (5 μM) in P80 buffer was mixed with 20 μM vinblastine and run with 0−0.5% DMSO to verify the reproducibility of spiral formation (solid lines; curves that peak near 28 S with an average S_w of 25.2 ± 0.91). We then added eribulin (cyan lines) or ER-076349 (blue lines) to solutions of vinblastine−tubulin spirals to measure the competition of these analogues with vinblastine. (A) $g(s)$ sedimentation coefficient distributions of vinblastine−tubulin mixtures titrated with erubulin. (B) Weight-average S_w values (±error) plotted vs total (□) eribulin or (△) ER-076349 added. The dotted horizontal line represents the extrapolated sedimentation coefficient of the tubulin heterodimer (see Figure 2B). The dashed and dashed−dotted lines represent simulations of vinblastine-induced spirals in the presence of a drug that sequesters tubulin into a weak (2.7×10^5 M^{-1}) and strong (2.7×10^8 M^{-1}) 1:1 complex, respectively. Sequestering alone clearly does not describe these competition data.

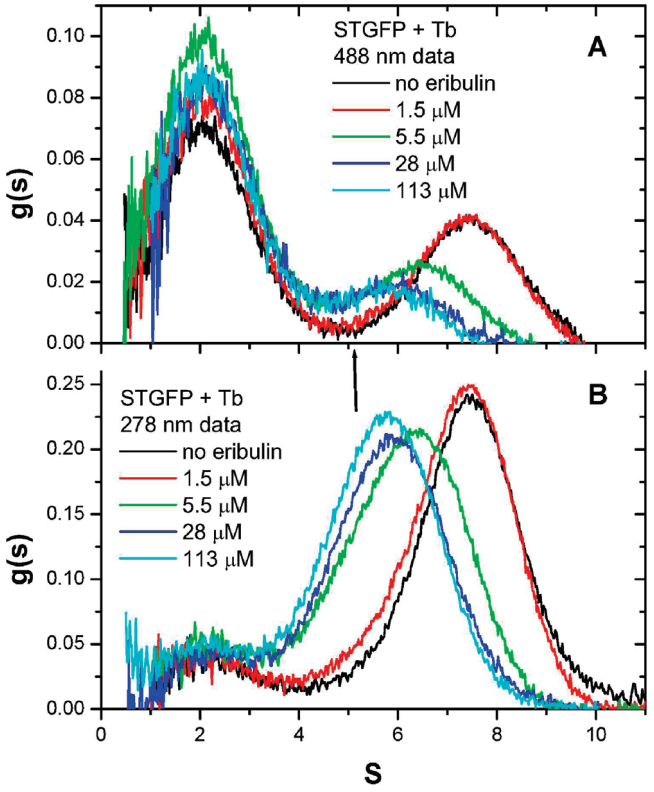

FIGURE 5: Sedimentation velocity $g(s)$ analysis of the effects of eribulin on stathmin−tubulin interactions. Data were collected on a mixture of 5 μM stathmin−eGFP and 5 μM tubulin at two wavelengths [(A) 488 and (B) 278 nm], and DCDT^{+2} $g(s)$ analysis is presented for all samples at both wavelengths. The free stathmin−eGFP construct is in excess, and the distributions appear as two zones reflecting the presence of the free stathmin−GFP complex and the $StTb_2$ complex. With increasing drug concentrations, the position of the reacting boundary corresponding to complex shifts to lower extents of association. With eribulin, the extent of reaction is dramatically weakened, consistent with formation of weak eribulin−tubulin complexes (indicated by the arrow).

competition was simulated by calculating the S_w for vinblastine-induced polymerization in the presence of a drug that forms a 1:1 tubulin complex (*26*−*28*). Two lines appear on the plot generated with weak (2.7×10^5 M^{-1}) and with strong (2.7×10^8 M^{-1}) 1:1 sequestering affinity. Neither line generates the steep substochiometric effect, nor do they match the rather shallow trend at higher drug concentrations. The substoichiometric effect thus requires a direct interaction with spirals. Direct interaction could mean eribulin and ER-076349 bind with high affinity to the interdimer interface, directly competing with vinblastine and weakening spiral formation by a direct or allosteric effect. Substoichiometric effects are common in the microtubule assembly field, and by analogy, we might also allow for capping of the exposed β-subunit at the plus ends and thus poison spiral growth by preventing tubulin addition. This would not necessarily require an affinity higher than 10^7 M^{-1} to be inhibitory and may be consistent with the shallow trend of the data at higher drug concentrations (see Discussion).

As an additional test of the mode of action of these halichondrin B analogues, we investigated the ability of eribulin and ER-076349 to disrupt the formation of a 1:2 stathmin−tubulin complex. Recently, Gigant et al. (*8*) reported the ability of vinblastine to incorporate into a stathmin−tubulin complex that also contained two molecules of colchicine. We have shown that stathmin competes for vinblastine-induced spiral formation (*39*, *41*). Results from Devred et al. (*40*) suggest binding of vinblastine to tubulin is enhanced 50-fold in the presence of stathmin, although our previous results for vinblastine binding suggest it is more like 2−5-fold (*17*, *18*) (see Discussion). Nonetheless, consistent with the effect of eribulin on tubulin and on vinblastine spirals, we anticipated eribulin would destabilize the stathmin−tubulin complex. The human stathmin used in these studies has an eGFP attached to the C-terminus, and thus, data were collected at two wavelengths (278 and 488 nm) to independently monitor the location of the stathmin in the sedimenting boundary. The results are presented in Figure 5, with the top panel corresponding to 488 nm data (stathmin−GFP) and the bottom panel corresponding to the 278 nm data (tubulin and stathmin−GFP). The addition of eribulin causes a dramatic shift in the $StTb_2$ complex zone, suggesting that eribulin inhibits stathmin−tubulin interaction. As with the tubulin alone data in Figure 1C, either eribulin sequesters stathmin-free tubulin or eribulin is incorporated into the $StTb_2$ complex destabilizing it. Notice that the region of the boundary corresponding to the complex seems to still be shifting to lower S values at the highest drug concentration. This suggests an approach of the boundary

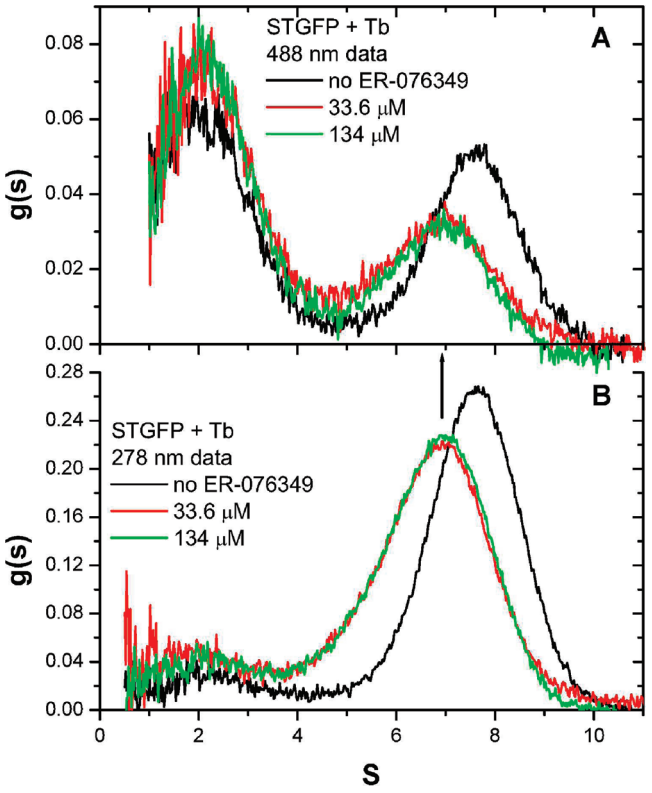

FIGURE 6: Sedimentation velocity $g(s)$ analysis of the effects of ER-076349 on stathmin−tubulin interactions. Data were collected on a mixture of 5 μM stathmin−eGFP construct and 5 μM tubulin at two wavelengths [(A) 488 and (B) 278 nm], and DCDT^{+2} $g(s)$ analysis is presented for all samples at both wavelengths. The free stathmin−GFP construct is in excess, and the distributions appear as two zones reflecting the presence of the free stathmin−GFP construct and the $StTb_2$ complex. With increasing drug concentrations, the position of the reacting boundary corresponding to the complex shifts to lower extents of association. With ER-076349, the reactions shifts less significantly than that of eribulin (indicated by the arrow), consistent with a weaker destabilizing effect on the $StTb_2$ complex.

to sequestered tubulin−drug complexes (the arrow). Thus, these data reflect the relative strength of stathmin and eribulin binding which implies competition between a 1:2 stathmin−tubulin complex and eribulin−tubulin complexes. Similar experiments were performed with ER-076349 (Figure 6) with data also collected at 488 and 278 nm. A similar result was obtained, although the shift was less dramatic than that in the eribulin data. At saturating amounts of ER-076349, on the basis of an absence of a shift in the boundary between 33 and 134 μM drug, the complex migrates at ~7 s. Like the effect on small tubulin oligomers (Figure 1C), this result suggested ER-076349 can incorporate into the $StTb_2$ complex and weaken complex stability.

A quantitative analysis of these results can be obtained by Sedanal fitting of the data to an ABCD or a 1:2 model to extract the apparent decrease in complex stability. The no drug controls (two sets of 278 and 488 nm data) were jointly fit to establish the energetics of the $StTb_2$ system. The best fit is a weak K_1 (0.345×10^4 M^{-1}) to form the 1:1 complex and a tight and cooperative K_2 (7.783×10^8 M^{-1}) to form the full 1:2 complex (Table 2). This result is supported by the 95% confidence intervals reported for the fit. [More computational details about this approach will be presented in separate publications on stathmin−tubulin interactions (*41*, *42*).] This K_1K_2 fit is only slightly better than a fit in which K_1 is constrained to 10^4 M^{-1}. Thus, to simplify the quantitative comparison, the drug data were individually fit to a constrained K_1 model to estimate the apparent reduction in K_2, $K_{2,app}$. A representative fit is shown in Figure 7, and the best-fit values are listed in Table 2. As described above, the eribulin data (Figure 5) suggest destabilization of the $StTb_2$ complex by either formation of eribulin−tubulin complexes or direct binding to the $StTb_2$ complex. The fitted data in Table 2 show a reduction in $K_{2,app}$ corresponding to 3.3 kcal/mol or a 475-fold decrease in binding affinity. The ER-076349 data suggest a 1.9 kcal/mol reduction in the stability of the $StTb_2$ complex corresponding to a 26-fold reduction in overall binding affinity. In both instances, the destabilized complex appears to be comprised of a 1:2:1 stathmin:tubulin:drug molar ratio that may also be in competition with drug-induced oligomers (see Discussion).

DISCUSSION

The major difference between these halichondrin B derivatives and vinblastine is that eribulin and ER-076349 mostly inhibit polymer formation rather than strongly inducing tubulin oligomer formation.[3] This conclusion is established by three experimental systems: tubulin oligomers alone (Figure 2), vinblastine-induced spirals (Figure 4), and formation of the stathmin−tubulin complex (Figure 5-7). In the first system, tubulin oligomer formation is inhibited by eribulin, and at low protein concentrations, the boundary runs with an S_w value corresponding to the tubulin heterodimer, indicated by the extrapolation of the S_w data for pure tubulin to zero protein concentration. If this represents sequestering, it implies eribulin has the ability to bind to half of the vinblastine site or domain on the heterodimer, either the α-chain or the β-chain, but probably not both since that would seem to predict formation of a complex with eribulin in the middle. Alternatively, the apparent K_{iso}, the propagation constant for oligomer formation in the presence of eribulin (Table 1), is at least 4−6-fold weaker than that of tubulin self-association alone. Both of these processes, sequestering and weak oligomer formation, may be occurring. A resolution requires an independent estimate of the affinity of eribulin for the tubulin heterodimer in the absence of oligomer formation, and this might be achievable in an SPR experiment where tubulin is linked to a matrix that prevents tubulin−tubulin interaction. Contrary to the results with eribulin, ER-076349 slightly enhances oligomer formation (Figure 2C and Table 1) and thus implies a weak stabilization (not necessarily weak binding) at or near the interdimer interface. This result is consistent with the concept of an adaptive binding site (*19*, *42*, *43*) where the interdimer interface can adjust topology to interact in slightly different ways with different drug moieties.[4] This is consistent with the polymorphic character of tubulin polymerization where microtubules, sheets, rings, spirals, and small oligomers can all be formed, mediated in part through interactions at the same site. In this case, the estimate of the K_{iso} value implies a direct role for ER-076349 in polymer formation. This is still an apparent value and does not directly inform us about drug binding, since

[3]It is worth noting that eribulin is not the first drug that acts as a global inhibitor of tubulin polymerization; maytansine is also known to bind competitively to the vinca alkaloid site with an affinity similar to that reported here (see Figure 4; $K_i = 0.5$ μM) and prevent nucleotide exchange and polymer formation (*47*). While maytansine proved to be too toxic and failed clinical trials (100−1000-fold more cytotoxic than vinblastine), newer derivatives are being targeted to tumors by attachment to monoclonal antibodies to take advantage of this cytotoxicity (*48*).

[4]This also predicts a small change in entropy or at least the absence of a large unfavorable entropy of binding (*20*, *49*, *50*).

Table 2: Summary of K_1, K_2, and $K_{2,app}$ Values for Stathmin Binding to Tubulin in the Presence of Varying Concentrations of Eribulin or ER-076349[a]

conditions	K_1 (M^{-1})	K_2 (M^{-1})	$\Delta\Delta G$ (kcal/mol)	rmsd
0.0 μM	1×10^4	2.852×10^8 (2.401, 3.428)	–	0.005995
	0.345×10^4 (0.279, 0.655)	7.783×10^8 (4.266, 9.327)	–	0.005872
[eribulin] (μM)	K_1 (M^{-1})	$K_{2,app}$ (M^{-1})	$\Delta\Delta G$ (kcal/mol)	rmsd
1.5	1×10^4	4.565×10^7	0.99	0.006981
5.5	1×10^4	2.069×10^6	2.67	0.006466
28	1×10^4	1.004×10^6	3.01	0.006814
113	1×10^4	5.684×10^5	3.37	0.006172
[ER-076349] (μM)	K_1 (M^{-1})	$K_{2,app}$ (M^{-1})	$\Delta\Delta G$ (kcal/mol)	rmsd
1.7	1×10^4	1.201×10^8	0.47	0.011213
6.7	1×10^4	7.681×10^6	1.96	0.012225
33	1×10^4	9.238×10^6	1.86	0.007206
134	1×10^4	9.922×10^6	1.83	0.006608

[a] The $\Delta\Delta G$ values are calculated relative to no drug. The $K_{2,app}$ values are apparent values because they reflect the influence of drug without directly incorporating drug binding into the fitting model. The K_1 and K_2 values for no drug conditions determined with Sedanal are reported with 95% confidence intervals.

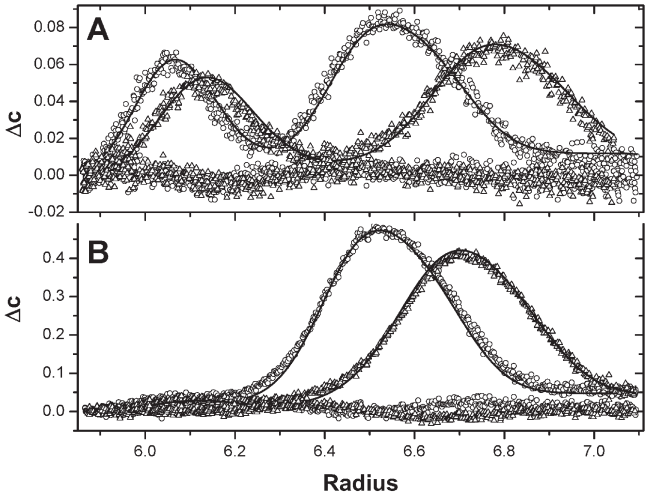

FIGURE 7: Sedanal (*29*) analysis of 1.5 μM eribulin inhibition of stathmin−tubulin interaction. The fits of the data are to an ABCD model involving the two-step formation of a weak 1:1 stathmin−tubulin complex ($K_1 = 10^4$ M^{-1}, held constant) and a strong and cooperative 1:2 stathmin−tubulin complex. In the presence of drug, the $K_{2,app}$ is fit to estimate the apparent weakening of the overall complex formation. This reflects the assumptions that eribulin and ER-076349 bind to and disrupt the tubulin interdimer interface in the 1:2 complex: (A) 488 nm data and (B) 278 nm data. Results for all conditions are listed in Table 2.

tight binding to the heterodimer could precede weak oligomer formation (see below). Independent measurements directly sensitive to a drug binding step are required to verify this.

The second experimental system supporting inhibition of tubulin polymer formation by eribulin and ER-076349 is a competition experiment with vinblastine-induced spiral formation. These experiments reveal that both eribulin and ER-076349 strongly inhibit spiral formation even at substoichiometric levels. This is not explained by sequestration of tubulin dimers (Figure 4) but rather requires direct interaction of the drug with vinblastine-induced spirals. Competition for the interdimer domain seems to require rapid exchange between drugs at interdimer binding sites. The similarity of the response of vinblastine spirals to these two drugs may thus reflect the fact that the apparent K_{iso} values in the presence of eribulin and ER-076349 (Table 1) are at least 3 orders of magnitude weaker than the vinblastine-induced K_{iso} [2.3×10^7 M^{-1} (*17*, *18*)]. This means if they exchange for vinblastine they weaken that interface site and cause spiral dissociation and a smaller size distribution. Thus, by copolymerizing with vinblastine, eribulin and ER-076349 weaken spiral formation. Neither set of S_w data returns to the heterodimer baseline value of 5.1 S at high drug concentrations (see Figure 4B). This must reflect the competition between the strong spiraling potential of vinblastine and the inhibitory activity of these analogues. Thus, even at high eribulin and ER-076349 concentrations, there must still be small vinblastine oligomers in solution. It is thus not clear that a strong binding affinity is required to explain the dramatic inhibition of vinblastine spiral formation by substoichiometric amounts of eribulin and ER-076349. These results may also reflect capping of spirals by binding to exposed β-subunit and preventing elongation to longer polymers. Thus, polymer and drug dynamics may also play a role. We are currently developing stochastic models to simulate copolymerization of drug-induced polymers to help interpret these data. Additional experiments with both sequestering drugs and weak vinca alkaloids may also be required to fully understand the nature of this competition reaction.

The third experimental system supporting inhibition of the formation of tubulin polymers by eribulin and ER-076349 involves the inhibition of formation of a 1:2 stathmin−tubulin complex. Eribulin causes nearly complete dissociation of the $StTb_2$ complex, although as discussed above this may reflect a combination of sequestering activity, weak drug-induced oligomer formation, and direct binding to and weakening of the $StTb_2$ complex of eribulin. The apparent changes in free energy reported in Table 2 reflect the sum total of these events. To test this conclusion, we can fit these AUC data to just a sequestering model, although since the drug has no absorbance we have no signal to constrain the free and bound drug fractions. Nonetheless, an ABCD model was modified via addition of a reaction representing sequestration of tubulin by eribulin. The values of K_1 and K_2 were fixed to the best-fit values in Table 2, and the total eribulin concentrations were also fixed to the values listed in Table 2. The global fit has significant systematics in some of the samples, consistent with errors in drug concentration, but the overall fit is surprisingly good for 10 data sets (a control and four

eribulin concentrations at two wavelengths). The best-fit value for the 1:1 reaction K is 2.7×10^5 M^{-1} with a global rmsd of 0.01526 (data not shown). Does this value make sense? If you take this 1:1 affinity and simulate the vinblastine results as vinca spirals competing with eribulin sequestering, it completely fails to match the data (the shallow dashed line in Figure 4B). Thus, we are forced to conclude eribulin must bind directly to both vinblastine spirals and the $StTb_2$ complex since sequestration alone cannot explain either result.

Consistent with the oligomer results and the vinblastine data, ER-076349 behaves in a similar manner, destabilizing the 1:2 stathmin−tubulin interaction, although less strongly than eribulin. This again implies an adaptive interaction in which the interdimer interface in the complex can adjust and accommodate ER-076349 binding but at a cost to the total stability of the now ternary complex (St−Tb_2−ER-076349).[5] [We cannot exclude the possibility of higher-order complexes, St−Tb_2−ER-076349_2. There is evidence for two potential drug binding sites in the St−Tb_2 complex as reported by Cormier et al. (*51*), where phompopsin A was shown to bind at the $\beta1-\alpha2$ interface and at the exposed $\beta2$ site. Given the potential mechanism proposed for eribulin, binding to a free β-site, we cannot exclude this possibility for ER-076349.] The St−Tb_2 $K_{2,app}$ values reported in Table 2 are reasonable estimates of overall stability assuming saturation of the ER-076349 binding site, which is implied by the superposition of the $g(s)$ distributions (Figure 6). The cellular implication of these results is that eribulin and ER-076349 compete with or mimic stathmin and sequester tubulin in a nonmicrotubule forming complex. This of course depends upon the relative intracellular concentration of the drug versus stathmin.

A cartoon is presented in Figure 8 with the various reactions discussed in these three experimental systems. The figure depicts the sequestration of tubulin by drug, the weak ability of tubulin and drugs to induce oligomers, the strong interaction of the ST−eGFP construct with tubulin to make a 1:2 complex, and the ability of both eribulin and ER-076349 to dissociate or weaken the $StTb_2$ complex by mass action or direct binding. While we prefer a model of drug binding to the interdimer interface, we cannot exclude additional binding to the exposed β-subunit in any of these complexes. Recently, Devred et al. (*40*) reported a similar thermodynamic cycle for interaction of tubulin with vinblastine and stathmin. They conclude from their ITC experiments that vinblastine binding to the interdimer interface is enhanced by the presence of stathmin. We agree that some of their numbers are K_{app} values and not intrinsic affinities. For example, the vinblastine binding to tubulin experiment measures K at a single set of concentrations and does not take into account the linkage between drug binding and ligand-induced oligomer formation. Thus, their value is underestimated (*17*−*19*). In addition, the stathmin−tubulin binding data are treated as a single set of sites, meaning K_1 and K_2 are equal or at least equivalent (Table 2) (*42*). This is clearly not the case in our analysis where $K_2/K_1 > 10^4$ (Table 2). Nonetheless, the appropriate value to use in their cycle may still be the midpoint of the reaction corresponding to $(K_1K_2)^{1/2}$ which is similar to their value (when corrected for conditions). Thus, we agree that the affinity of vinblastine for the interdimer interface may be similar in spirals and in the $StTb_2$ complex, although a 50-fold increase may be too large an estimate. A correction for a $K_{intrinsic}$ rather than a K_{app} value for vinblastine binding to spirals probably decreases their estimate by approximately 10-fold.

What are the implications of these results for interactions of the drug with microtubules? Jordan et al. (*52*) demonstrated that eribulin suppresses microtubule growth but not shortening, rescue, or catastrophe. This is consistent with eribulin binding to polymer ends. They only looked at plus ends, so we can conclude the drug binds to the β-subunit which is exposed at the plus end. It also implies that eribulin at the concentrations used (100 nM) has little or no ability to bind to the microtubule lattice, at interdimer interfaces; otherwise, disassembly rates would be affected. We can only speculate that there will be a pool of free drug and drug complexes that can add directly to microtubule ends and block or poison assembly. Thus, unlike colchicine (see ref *53*), we suggest the path for drug binding to microtubules can occur by drug or a drug−tubulin complex binding to the exposed β-subunit at the plus end of the microtubule. We also anticipate a difference at the plus and minus endd since binding of an eribulin complex to the plus end poisons that end toward further growth, while binding to the minus end is a low-affinity event due to the mode of action of eribulin and thus should be less sensitive to substoichiometric behavior. What can we anticipate for the effects of ER-076349 on microtubule dynamics? Since this analogue can be incorporated into oligomers, vinblastine spirals, and stathmin−tubulin complexes in a manner similar to that of eribulin, we anticipate that at comparable concentrations ER-076349 will inhibit microtubule growth while not displaying an effect on disassembly rates, rescue, or catastrophe.

Jordan et al. (*52*) also concluded eribulin inhibited microtubule growth by sequestration of tubulin into aggregates based on the presence of irregular aggregates in EM. We agree with this in principle, but the oligomers are clearly small under our conditions. (Large irregular EM aggregates seen may represent denatured tubulin present in all tubulin solutions, especially at higher temperatures.) Most vinca alkaloid binding drugs inhibit both growth and shortening, consistent with binding to microtubule ends, formation of an alternate polymer lattice at the end, and thus disruption of both growth (or further addition of subunits) and disassembly (or stabilization of microtubule ends by the presence of bound drug). In addition, vinblastine has been shown to bind to the microtubule lattice by cyro-EM and traditional binding methods (*54*−*56*). This conclusion is supported by the recent docking studies of Dabydeen et al. (*15*), who suggested that eribulin disrupts the dimer−dimer interface in the stathmin−tubulin crystal structure. This is exactly what we observed for eribulin (see Figure 5) and similar to what is also observed for ER-076349 (see Figure 6). Dabydeen et al. conclude that unlike vincristine and vinblastine, eribulin should bind to subunits or small, highly unstable tubulin polymers.[6] It would be helpful to

[5] This same observation, that ER-076349 destabilizes the $StTb_2$ complex, can be asked about other drugs. This is the question posed in the discussion about vinblastine being observed in the crystal structure of a 1:2 stathmin-like domain and tubulin complex (*6*). Does vinblastine binding stabilize or destabilize the $StTb_2$ complex? The quantitative challenge in this case is the competition between spirals, the 1:2 $StTb_2$ complex, and vinblastine binding to that complex. The $StTb_2$ crystal structure also has two colchicine molecules at the intradimer interface, and we have measured the stability of this ternary complex (St−Tb_2−Col_2) by similar quantitative AUC methods and found it to be destabilized relative to the $StTb_2$ complex by 1.1−1.5 kcal/mol (*39*). The relative stability of these complexes has potential implications for drug efficacy, especially in cell lines or tumors in which the levels of microtubule regulators vary.

[6] The only minor caveat to these docking studies is that the structure contains two bound colchicines, a bound vinblastine, and a bound stathmin-like domain, any one of which could perturb the tubulin−tubulin interface in a way to make this a nontypical interdimer interface. Given the adaptability we propose above, this may in fact be the typical case, which is an ensemble of slightly different structures stabilized by either drug binding, alternate polymer formation, or both.

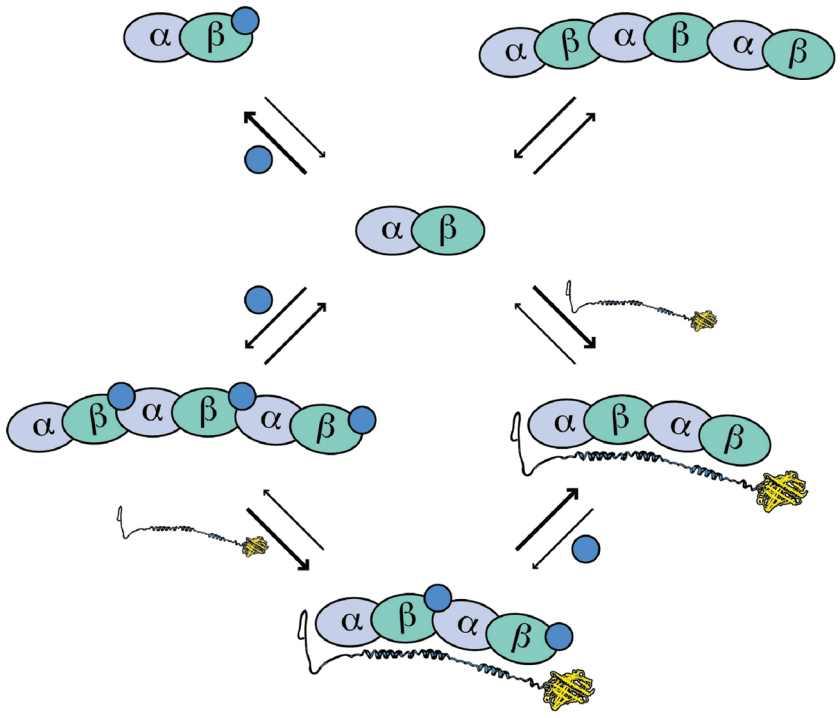

FIGURE 8: Cartoon with the various reactions discussed depicting the sequestration of tubulin, the weak ability to induce oligomers, the strong interaction of the ST−eGFP construct with tubulin to make a 1:2 complex, and the ability of both eribulin and ER-076349 to dissociate or weaken the $StTb_2$ complex. The reaction schemes allow sequestration or weak oligomer formation by either drug (blue circles). Either drug may destabilize $StTb_2$ by sequestration, by weak oligomer formation, or by direct binding to the complex. Finally, since a 1:1 sequestering mechanism suggests binding to an exposed β-subunit and the vinblastine inhibition data suggest direct binding to vinca-induced spirals, the reaction schemes allow for capping of oligomers as well as the $StTb_2$ complex. This would affect polymer growth as well as complex stability by an allosteric mechanism. The relative strength of each reaction is indicated by the size of the arrows. Note that stathmin is represented by a folded structure, although we anticipate free stathmin is intrinsically disordered and induced to fold upon binding to tubulin.

compare molecular dynamics simulations on ER-076349 with eribulin to see if the docking can mimic or predict the relative stabilizing influence of ER-076349 over eribulin in both the tubulin−tubulin polymers (Figure 1) and the stathmin−tubulin complex (Figures 5 and 6).

Halichondrin B analogues are a class of unique anticancer compounds that have been developed from marine natural products into synthetic derivatives that are undergoing phase III clinical trials (*43*−*46*). While the success of a cancer drug is difficult to predict, there has been extensive justification for investigations into the physical and mechanistic basis of action for many of these compounds (*1*, *2*, *18*, *20*, *38*). Our previous studies (*16*−*18*, *27*, *28*, *38*) focused on determining the overall mechanism and energetics of vinca alkaloid-induced tubulin spirals and then using those affinities as predictors of IC_{50} values and clinical doses (*38*). For vinca alkaloids, the overall spiraling potential, measured as an affinity or a free energy, inversely correlates with IC_{50} values and clinical doses (*2*, *38*), with the strongest drugs being effective at the lowest doses and the weakest drugs being effective at the highest doses. These data correspond to a 500-fold range in affinities that correlates to a 32-fold range in IC_{50} values [L1210 leukemia cell line (*2*, *38*)] and a 160-fold range in clinical doses (*2*). In the vinblastine competition measurements presented here, eribulin and ER-076349 are estimated to bind directly to the spiral polymer and disrupt assembly. The disruption comes from the weak tubulin spiraling potential of these drugs corresponding to $0.3-4.6\times10^4\ M^{-1}$. This is inconsistent with the 4.1-fold higher average IC_{50} values reported in the literature for vinblastine relative to eribulin (*9*, *13*). In addition, vinblastine has a clinical dose of ~8 mg/m^2. The clinical dose for eribulin from a phase II trial in metastatic breast cancer is 1.4 mg/m^2 using a day 1,8 Q21 dosing regimen (*38*, *39*). Thus, both of these comparisons are inconsistent with a thermodynamic approach that inversely correlates in vitro spiraling with clinical dose. This seems to suggest the potency of these drugs is due to their disruptive effect on multiple tubulin interaction partners rather than on their ability to sequester tubulin into a spiral complex. Specifically, one can speculate that the inhibition of formation of the stathmin−tubulin complex by eribulin represents targeting stathmin in vivo and may explain the unique clinical profile of these drugs.

This is one of the first reports to demonstrate both allosteric and competitive drug effects with antimitotic drugs and microtubule regulatory factors. We have proposed on numerous occasions (*1*, *2*, *17*) that antimitotic drugs can be viewed as mimics of microtubule regulatory factors; this may be in part their biological function in the plants and organisms in which they are found. Consistent with this view, Cormier et al. (*57*) recently reported that the PN2-3 domain of CPAP (also named CENPJ), a centrosomal protein, sequesters tubulin into a 1:1 complex, thus making eribulin a mimic of PN2-3. Like eribulin, PN2-3 inhibits vinblastine-induced assembly, inhibits the binding of stathmin, and is proposed to bind on the β-subunit of tubulin at the interdimer interface. Like maytansine (*38*) and eribulin (*15*), PN2-3 also inhibits GTPase activity and nucleotide exchange. In terms of clinical utility, the inhibition or allosteric disruption of the microtubule regulator stathmin may have implications for drug efficacy as well as tissue specific or tumor specific selectivity. Many transformed cells and tumors are reported to have altered levels of stathmin (*58*). This alone is known to impact IC_{50} values

in cells by destabilizing microtubules (*1*, *2*, *59*). If a drug also targets stathmin activity in addition to microtubule dynamics, the outcome may be significantly different than disruption of dynamics alone. This mechanism alone may account for a different phenotype exhibited by eribulin and ER-076349 against cancer cells and tumors than for example taxanes (*13*, *14*). In terms of future development, specific targeting of these tubulin−regulatory factor interactions may be possible within the context of further design of these compounds. Alternatively, in combination with analysis of molecular markers or unique molecular activities, the ability of these compounds to target selective interactions may prove to be useful clinically against certain tumors or stages of disease (*20*). Our laboratory has recently created stable stathmin knocked down cell lines (2-fold) by siRNA in a breast cancer cell line and initially observed sensitivity to paclitaxel. Subsequent clones, however, were resistant to paclitaxel or had no change in IC_{50} values. This appears to be due to compensating changes in both MAP4 and tubulin isotype levels (S. Lobert and J. J. Correia, unpublished observations). Nonetheless, it would be of interest to investigate the response to drugs that are known to also target stathmin−tubulin interactions in these cell lines. It would test the hypothesis that disruption of stathmin sequestering activity contributes in a unique way to drug toxicity. Given the function of CPAP, it is conceivable that eribulin has unique effects on centriole assembly and centrosomal function. Similar approaches could be used for other regulatory factors like MAP4 or MCAK. To integrate our understanding of drug activity, we are also developing microtubule dynamic simulation software that incorporates these specific regulatory mechanisms and allows us to investigate drug-dependent effects on dynamics, microtubule regulation, and cytotoxicity (M. Schilstra, S. Martin, and J. J. Correia, manuscript in preparation) (*60*).

ACKNOWLEDGMENT

All experiments were conducted in the UMMC AUC Facility. This is publication 47 from the UMMC AUC Facility. We thank Bruce Littlefield for helpful discussions and Sharon Lobert for critiquing the manuscript. We thank David Brown for help with the stathmin−eGFP cloning.

REFERENCES

1. Correia, J. J., and Lobert, S. (2001) Physiochemical Aspects of Tubulin-Interacting, Antimitotic Drugs. *Curr. Pharm. Des. 7*, 1213–1228.
2. Correia, J. J., and Lobert, S. (2008) Molecular Mechanisms of Microtubule Acting Cancer Drugs. In Microtubules in Health and Disease (Fojo, T., Ed.) pp 21−46, Humana Press, Totowa, NJ.
3. Nogales, E., Wollf, S. G., and Downing, K. H. (1998) Structure of the $\alpha\beta$ tubulin dimer by electron crystallography. *Nature 391*, 199–203.
4. Amos, L. A., and Lowe, J. (1999) Taxol stabilizes microtubule structure. *Chem. Biol. 6*, R65–R69.
5. Downing, K. H., and Nogales, E. (1998) New insights into microtubule structure and function from the atomic model of tubulin. *Eur. Biophys. J. 27*, 431–436.
6. Ravelli, R. B. G., Gigant, B., Curmi, P. A., Jourdain, I., Lachkar, S., Sobel, A., and Knossow, M. (2004) Insight into tubulin regulation from a complex with colchicines and a stathmin-like domain. *Nature 428*, 198–202.
7. Andreu, J. M., Wagenknecht, T., and Timasheff, S. N. (1983) Polymerization of the tubulin-colchicine complex: Relationship to microtubule assembly. *Biochemistry 22*, 1556–1566.
8. Gigant, B., Wang, C., Ravelli, R. B. G., Roussi, F., Steinmetz, M. O., Curmi, P. A., Sobel, A., and Knossow, M. (2005) Structural basis for the regulation of tubulin by vinblastine. *Nature 435*, 519–527.
9. Bai, R., Paull, K. D., Herald, C. L., Malspeis, L., Pettit, G. R., and Hamel, E. (1991) Halichondrin B and Homohalichondrin B, Marine Natural Products Binding in the Vinca Domain of Tubulin. *J. Biol. Chem. 266*, 15882–15889.
10. Luduenã, R. F., Roach, M. C., Prasad, V., and Pettit, G. R. (1993) Interaction of halichondrin B and homohalichondrin B with bovine brain tubulin. *Biochem. Pharmacol. 45*, 421–427.
11. Bai, R., Cichacz, Z. A., Herald, C. L., Pettit, G. R., and Hamel, E. (1993) Spongistatin 1, a highly cytotoxic, sponge-derived, marine natural product that inhibits mitosis, microtubule assembly, and the binding of vinblastine to tubulin. *Mol. Pharmacol. 44*, 757–766.
12. Hamel, E. (1992) Natural products which interact with tubulin in the *vinca* domain: Maytansine, rhizoxin, phomopsin A, dolastatins 10 and 15 and Halichondrin B. *Pharmacol. Ther. 55*, 31–51.
13. Towle, M. J., Salvato, K. A., Budrow, J., Wels, B. F., Kuznetsov, G., Aalfs, K. K., Welsh, S., Zheng, W., Seletsky, B. M., Palme, M. H., Habgood, G. J., Singer, L. A., Dipietro, L. V., Wang, Y., Chen, J. J., Quincy, D. A., Davis, A., Yoshimatsu, K., Kishi, Y., Yu, M. J., and Littlefield, B. A. (2001) In Vitro and In Vivo Anticancer Activities of Synthetic Macrocyclic Ketone Analogues of Halichondrin B. *Cancer Res. 61*, 1013–1021.
14. Kuznetsov, G., Towle, M. J., Cheng, H., Kawamura, T., TenDyke, K., Liu, D., Kishi, Y., Yu, M. J., and Littlefield, B. A. (2004) Induction of morphological and biochemical apoptosis following prolonged mitotic blockage by Halichondrin B macrocyclic ketone analog E7389. *Cancer Res. 64*, 5760–5766.
15. Dabydeen, D. A., Burnett, J. C., Bai, R., Verdier-Pinard, P., Hickford, S. J. H., Pettit, G. R., Blunt, J. W., Munro, M. H. G., Gussio, R., and Hamel, E. (2006) Comparison of the Activities of the Truncated Halichondrin B Analog NSC 707389 (E7389) with Those of the Parent Compound and a Proposed Binding Site on Tubulin. *Mol. Pharmacol. 70*, 1866–1875.
16. Lobert, S., and Correia, J. J. (2007) Methods for studying vinca alkaloid interaction with tubulin (Zhou, J., Ed.) Chapter 18, pp 261−280, Humana Press, Totowa, NJ.
17. Lobert, S., and Correia, J. J. (2000) Energetics of Vinca Alkaloid Interactions with Tubulin. *Methods Enzymol. 323*, 77–103.
18. Lobert, S., Ingram, J. W., and Correia, J. J. (2007) The Thermodynamics of Vinca Alkaloid-Induced Tubulin Spiral Formation. *Biophys. Chem 126*, 50–58.
19. Na, G. C., and Timasheff, S. N. (1985) Measurement and analysis of ligand-binding isotherms linked to protein self-association. *Methods Enzymol. 117*, 459–519.
20. Arkin, M. R., and Wells, J. A. (2004) Molecular Inhibitors of Protein-Protein interactions: Progressing towards the dream. *Nat. Rev. Drug Discovery 3*, 301–317.
21. Williams, R. C., Jr., and Lee, J. C. (1982) Preparation of tubulin from brain. *Methods Enzymol. 85*, 376–385.
22. Correia, J. J., Baty, L. T., and Williams, R. C., Jr. (1987) The Mg^{+2}-Dependence of Guanine Nucleotide Binding to Tubulin. *J. Biol. Chem. 262*, 17278–17284.
23. Detrich, H. W., III., and Williams, R. C., Jr. (1978) Reversible dissociation of the dimer of tubulin from bovine brain. *Biochemistry 17*, 3900–3907.
24. Penefsky, H. S. (1979) A centrifuged-column procedure for the measurement of ligand binding by beef heart F1. *Methods Enzymol. 56*, 527–531.
25. Pyles, E., and Bane Hastie, S. (1993) Effect of the B Ring and the C-7 Substituent on the Kinetics of Colchicinoid-Tubulin Associations. *Biochemistry 32*, 2329–2336.
26. Correia, J. J. (2000) The Analysis of Weight Average Sedimentation Data. *Methods Enzymol. 321*, 81–100.
27. Sontag, C. A., Stafford, W. F., and Correia, J. J. (2004) A Comparison of Weight Average and Direct Boundary Fitting of Sedimentation Velocity Data for Indefinite Polymerizing Systems. *Biophys. Chem. 108*, 215–230.
28. Correia, J. J., Sontag, C. A., Stafford, W. F., and Sherwood, P. J. (2005) Models for Direct Boundary Fitting of Indefinite Ligand-Linked Self-Association. In Analytical Ultracentrifugation: Techniques and Methods (Scott, D., Harding, S., and Rowe, A., Eds.) pp 51−63.
29. Philo, J. S. (2006) Improved methods for fitting sedimentation coefficient distributions derived by time-derivative techniques. *Anal. Biochem. 354*, 238–246.
30. Fukuda, H., Arai, M., and Kuwajima, K. (2000) Folding of green fluorescent protein and the cycle3 mutant. *Biochemistry 39*, 12025–12032.
31. Stafford, W. F., and Sherwood, P. J. (2004) Analysis of heterologous interacting systems by sedimentation velocity: Curve fitting algorithms for estimation of sedimentation coefficients, equilibrium and kinetic constants. *Biophys. Chem. 108*, 231–243.

32. Lu, S., and Stafford, W. S. (1995) An Optical Thermometer for Direct Measurement of Cell Temperature in the Beckman Instruments XL-A Analytical Ultracentrifuge. *Anal. Biochem. 224*, 199–202.
33. Lee, J. C., Frigon, R. P., and Timasheff, S. N. (1973) The chemical characterization of calf brain microtubule protein subunits. *J. Biol. Chem. 248*, 7253–7262.
34. Lee, J. C., and Timasheff, S. N. (1974) Partial specific volumes and interactions with solvent components of proteins in guanidine hydrochloride. *Biochemistry 13*, 257–265.
35. Laue, T. M., Shah, B. D., Ridgeway, T. M., and Pelletier, S. L. (1992) in Analytical Ultracentrifugation in Biochemistry and Polymer Sciences (Harding, S. E., Rowe, A. J., and Horton, J. C., Eds.) pp 90−125, Royal Society of Chemistry, Cambridge, U.K.
36. Patterson, G., Day, R. N., and Piston, D. (2001) Fluorescent protein spectra. *J. Cell Sci. 114*, 837–838.
37. Kneen, M., Farinas, J., Li, Y., and Verkman, A. S. (1998) Green fluorescent protein as a noninvasive intracellular pH indicator. *Biophys. J. 74*, 1591–1599.
38. Lobert, S., Fahy, J., Hill, B. T., Duflos, A., Entievant, C., and Correia, J. C. (2000) Vinca Alkaloid-Induced Tubulin Spiral Formation Correlates with Cytotoxicity in the Leukemic L1210 Cell Line. *Biochemistry 39*, 12053–12062.
39. Sontag, C. (2003) Quantitative Studies of Proteins that Interact with Tubulin by Analytical Ultracentrifugation. Ph.D. Thesis, University of Mississippi Medical Center, Jackson, MS.
40. Devred, F., Tsvetkov, P. O., Barbier, P., Allegro, D., Horwitz, S. B., Makarov, A. A., and Peyrot, V. (2008) Stathmin/OP18 is a novel mediator of vinblastine activity. *FEBS Lett. 582*, 248–388.
41. Alday, P. H. (2009) Use of Fluorescently Labeled Proteins in Quantitative Sedimentation Velocity Studies of Heterogeneous Biomolecular Interactions. Ph.D. Thesis, University of Mississippi Medical Center, Jackson, MS.
42. Correia, J. J., Alday, P. H., Sherwood, P. J., and Stafford, W. F. (2009) Effect of Kinetics on Sedimentation Velocity Profiles and the Role of Intermediates. Methods in Enzymology, Computer Methods, Part B (Johnson, M. L., and Brandt, L., Eds.) (in press).
43. Simmons, T. L., Andrianasolo, E., McPhal, K., Flatt, P., and Gerwock, W. H. (2005) Marine natural products as anticancer drugs. *Mol. Cancer Ther. 4*, 333–342.
44. Towle, M. J., Salvato, K. A., Budrow, J., Wels, B., Aalfs, K. K., Zheng, W., Seletsky, B. M., Palme, M. H., Habgood, G. J., Singer, L. A., DiPietro, L. V., Wang, Y., Chen, J. J., Lydon, P. J., Quincy, D. A., Kishi, Y., Yoshimatsu, K., Yu, M. J., and Littlefield, B. A. (2001) In vivo anticancer activity of synthetic halichondrin B macrocyclic ketone analogs ER-076349 and ER-086526 correlates with ability to induce irreversible mitotic blocks. Annual Meeting of the American Association for Cancer Research, New Orleans, LA, March 24−28, 2001 (Abstract 1976).
45. Vahdat, L. T., Pruitt, B., Fabian, C. F., Rivera, R. R., Smith, D. A., Tan-Chiu, E., Wright, J., Tan, A. R., DaCosta, N. A., Chuang, E., Smith, J., O'Shaughnessy, J., Shuster, D. E., Meneses, N. L., Chandrawansa, K., Fang, F., Cole, P. E., Ashworth, S., and Blum, J. L. (2009) Phase II Study of Eribulin Mesylate, a Halichondrin B Analog, in Patients With Metastatic Breast Cancer Previously Treated With an Anthracycline and a Taxane. *J. Clin. Oncol. 27*, doi: 10.1200/JCO.2008.17.7618.
46. Jimeno, A. (2009) Eribulin: Rediscovering Tubulin as an Anticancer Target. *Clin. Cancer Res. 15*, 3903–3905.
47. Huang, A. B., Lin, C. M., and Hamel, E. (1985) Maytansine inhibits nucleotide binding at the exchangeable site of tubulin. *Biochem. Biophys. Res. Commun. 128*, 1239–1246.
48. Widdison, W. C., Wilheim, S. D., Cavanagh, E. E., Whiteman, K. R., Leece, B. A., Kovtun, Y., Goldmacher, V. S., Xie, H., Steeves, R. M., Lutz, R. J., Zhao, R., Wang, L., Blattler, W. A., and Chari, R. V. J. (2006) Semisynthetic maytansine analogues for the targeted treatment of cancer. *J. Med. Chem. 49*, 4392–4408.
49. Hyde, J., Braisted, A. C., Randal, M., and Arkin, M. R. (2003) Discovery and characterization of cooperative ligand binding in the adaptive region of interleukin-2. *Biochemistry 42*, 6475–6483.
50. Arkin, M. R., Randal, M., DeLano, W. L., Hyde, J., Luong, T. N., Oslob, J. D., Raphael, D. R., Taylor, L., Wang, J., McDowell, R. S., Wells, J. A., and Braisted, A. C. (2003) Binding of small molecules to an adaptive protein:protein interface. *Proc. Natl. Acad. Sci. U.S.A. 100*, 1603–1608.
51. Cormier, A., Marchand, M., Ravelli, R. B. G., Knossow, M., and Gigant, B. (2008) Structural insight into the inhibition of tubulin by vinca domain peptide ligands. *EMBO Rep. 9*, 1101–1106.
52. Jordan, M. A., Kamath, K., Manna, T., Okouneva, T., Miller, H. P., Davis, C., Littlefield, B. A., and Wilson, L. (2005) The primary antimitotic mechanism of action of the synthetic halichondrin E7389 is suppression of microtubule growth. *Mol Cancer Ther. 4*, 1086–1095.
53. Skoufias, D. A., and Wilson, L. (1992) Mechanism of inhibition of microtubule polymerization by colchicine: Inhibitory potencies of unliganded colchicine and tubulin-colchicine complexes. *Biochemistry 31*, 738–746.
54. Santarella, R. A., Correia, J. J., Lobert, S., and Hoenger, A. (2005) Cryo EM studies of effects on microtubule structure by vinblastine-tau. *Mol. Biol. Cell Suppl. 16*, 957 (CDRom).
55. Jordan, M. A., Margolis, R. L., Himes, R. H., and Wilson, L. (1986) Identification of a distinct class of vinblastine binding sites on microtubules. *J. Mol. Biol. 187*, 61–73.
56. Singer, W. D., Jordan, M. A., Wilson, L., and Himes, R. H. (1989) Binding of vinblastine to stabilized microtubules. *Mol. Pharmacol. 36*, 366–370.
57. Cormier, A., Clement, M. J., Knossow, M., Lachkar, S., Savarin, P., Toma, F., Sobel, A., Gigant, B., and Curmi, P. A. (2009) The PN2-3 domain of CPAP implements a novel mechanism for tubulin sequestration. *J. Biol. Chem. 284*, 6909–6917.
58. Mistry, S. J., Bank, A., and Atweh, G. F. (2005) Targeting stathmin in prostate cancer. *Mol. Cancer Ther. 4*, 1821–1829.
59. Cabral, F. (2008) Mechanisms of Resistance to Drugs that Interfere with Microtubule Assembly. In Microtubules in Health and Disease (Fojo, T., Ed.) pp 337−356, Humana Press, Totowa, NJ.
60. Schilstra, M. J., Martin, S. R., and Correia, J. J. (2009) Comparison of Microtubule Dynamics for A- and B-Lattice Geometries. *Biophys. J.,* 107 (Abstract 2598).